Molecular Dynamics Simulations of Adipocyte Lipid-Binding Protein: Effect of Electrostatics and Acyl Chain Unsaturation

Marvin R. Rich*,‡ and John Spencer Evans§

Departments of Biology and Chemistry, New York University, Washington Square, New York, New York 10003

Received July 12, 1995; Revised Manuscript Received October 31, 1995⊗

ABSTRACT: Molecular dynamics (MD) simulations have been performed on adipocyte lipid-binding protein, using the apo and holo forms, bound with stearic and oleic acid. The contribution of electrostatics to protein dynamics and ligand stabilization was assayed by perturbing the electrostatic charge of Arg106 and Arg126 (positive → neutral) and the fatty acid (132H) headgroup (negative → neutral). MD simulations for charged holo forms demonstrated significantly greater electrostatic binding energy and a more stabilized hydrogen bond network than simulations performed using neutral forms. Electrostatics, however, appeared to have little effect on fatty acid behavior, *e.g.*, fluctuation of the dihedral head group; number of dihedral transitions within the acyl chain; and change in the end-to-end distance for fatty acid. Instead, fatty acid behavior appeared to be dictated by the presence or absence of an unsaturated bond within the acyl chain. A significantly greater number of transitions were observed during MD simulations in oleic than stearic acid. In addition, significantly greater fluctuation was observed for oleic acid, within the C2 headgroup and C9 and C11 dihedrals (which lie adjacent to the olefin bond of oleic acid). The dynamic behavior of the acyl chain may thereby be more a property of van der Waals contact, and the degree of acyl chain unsaturation, than a function of electrostatics. In the absence of fatty acid, an increase in distance between guanidino carbon centered atoms of Arg126 and Arg106 was observed during MD simulations of the charged apo form. This effect not observed with the neutral apo form or in any of the holo complexes and, presumbably, was a result of repulsion between the negatively charged arginine sidechains. Conserved waters reflected substantially lower mean-square displacement (msd) in all simulations, except the neutral apo form. This suggests that the presence of either charged amino acids or lipid provides increased order for water within the binding pocket. These results provide a dynamic perspective of the interactive nature within the FABP binding pocket regulated in a complex manner by the electrostatics within the binding cavity, acyl chain structure and behavior, and water energetics.

Lipid−protein interactions are ubiquitous to living systems. They are associated with energy and signal transduction mechanisms (Bienvenue *et al*., 1984; McPhail *et al.*, 1984; Veerkamp *et al.*, 1991) and are important to numerous cytosolic and membrane-bound processes (Prescott *et al*., 1990; Abramson *et al.*, 1991; Cremel *et al.*, 1993). An interesting model for studying lipid−protein interactions is the adipocyte lipid-binding protein, or ALBP.[1] ALBP is a member of a protein class that bind lipid-like molecules such as fatty acids and retinoid compounds (Banaszak *et al.*, 1994, and references therein). The postulated role of ALBP is that of a mediator of intracellular solubilzation and transport of fatty acids in adipocytes. The crystal structures of the apo and holo forms of ALBP, bound with saturated and unsaturated fatty acid, have recently been reported (Xu *et al.*, 1992, 1993; LaLonde *et al*., 1994a). These studies have shown that the structure of ALBP is comprised of the following: (1) Ten antiparallel β-strands (denoted as βA−βJ); these β-sheet domains are organized into two nearly orthogonal β-sheets, resulting in a barrel structure that surrounds an internal ligand-binding cavity. βA and βB domains are separated by a helix−loop−helix motif; the remaining β-strands are joined via loop or turn regions. A gap is present between two antiparallel strands βD and βE where no main-chain hydrogen bonds exist. (2) Two α-helices (α1, α2) that are located on the surface of one open end of the barrel (Banaszak *et al.*, 1994); these helices comprise the helix−loop−helix motif which joins βA with βB.

Of interest is the nature of the interactions between the fatty acid and the protein binding cavity. Obviously, a better understanding of these interactions may help us define the structure−function relationships of ALBP. The ALBP ligand-binding cavity is lined by 41 amino acids which have one or more sidechain atoms in contact with the pocket. The polar end of the fatty acid ligand is bound within this cavity; a portion of the fatty acid acyl chain extends outside the cavity. The volume of the cavity in the apo form of ALBP has been estimated at 600 Å^3 (Levitt & Banaszak, 1992). Although the cavity contains arginine and lysine, there is no evidence from recent X-ray crystallographic studies that these residues possess specific counterions. From the available structural data, binding of the fatty acid within the

* Author to whom correspondence should be addressed.
‡ Department of Biology.
§ Department of Chemistry.
⊗ Abstract published in *Advance ACS Abstracts,* January 1, 1996.
[1] Abbreviations: MD: molecular dynamics; NVT: constant number of particles, volume, and temperature; DPPC: dipalmitoylphosphatidylcholine; ALBP: adipocyte lipid-binding protein; ps: picoseconds; FA: fatty acid; FABP: fatty acid binding protein; apo: apoprotein form; Stear-C: ALBP−stearate complex, charged form; Stear-N: ALBP−stearate complex, neutral form; Oleic-C: ALBP−oleate complex, charged form; Oleic-N: ALBP−oleate complex, neutral form; WAT: specifically-bound crystallographic water molecules; CVFF: consistent valence forcefield; msd: mean-square displacement; C-C: carbon−carbon rotamer or dihedral.

0006-2960/96/0435-1506$12.00/0

cavity appears to be the result of a network of hydrogen bonds between four species: (1) the fatty acid carboxylate group, (2) two guanidino groups from Arg106 and Arg126, (3) the hydroxyl group from Tyr128, and (4) an intervening water molecule located between the carboxylate group and Arg106.

Moreover, both the fatty acid carboxylate and the guanidino groups are charged, which may further stabilize the fatty acid headgroup within the cavity via electrostatic interactions. One other feature of the binding cavity is the presence of 10 conserved water molecules (Banaszak *et al.*, 1994), whose role in fatty acid stabilization is unknown. Both saturated (palmitic, 16:0; stearate, 18:0) and unsaturated (oleic, 18:1) fatty acids bind to ALBP in a slightly bent conformation that contains several *gauche* conformers (Xu *et al.*, 1993; LaLonde *et al*., 1994a). It is possible that the presence of conserved waters, and the fatty acid conformational state, may be key factors in stabilizing the fatty acid within the cavity.

Little is known about the dynamic motion of the fatty acid within the pocket or whether such motion may affect ligand stability. When bound to protein, there is a trend toward increasing temperature factors of carbon atoms (in either stearic or oleic acids) as one goes from the carboxylate to the hydrocarbon end (Xu *et al*., 1993). Increased disorder as one moves along the acyl chain toward the center of a bilayer has been demonstrated in computer simulations using lipids containing saturated acyl chains (De Loof *et al*., 1991; Venable *et al*., 1993). In the case of ALBP bound with unsaturated fatty acid (18:1) there appears to be no atypical values for temperature factors for the region associated with the double bond, or the headgroup of oleic acid. In contrast, computer simulations of lipid model systems containing unsaturated acyl chains show increased motion within the double-bond region (Heller *et al.*, 1993) and associated with the lipid headgroup (Slater *et al.*, 1993). Information pertaining to the dynamic motion of the acyl chain can provide insight into factors which affect ligand binding.

To address the issues of acyl chain conformation, conserved water molecules, and binding cavity−fatty acid interactions, we have performed NVT (constant volume and temperature) molecular dynamics (MD) simulations, using the adipocyte lipid-binding protein (ALBP) as our model system. We have chosen this system because of the recent availability of the crystal structures for both the apo form and the stearic- and oleic-bound holo forms. Since stearic and oleic acids have the same carbon chain length but differ only in the degree of saturation, we can perform time-dependent comparisons of both protein−ligand complexes and examine acyl chain conformational differences that may arise due to the presence of an alkene bond. Furthermore, we can determine the effects of each fatty acid ligand on ALBP backbone and side-chain dynamics, and, the dynamics of the conserved water molecules which comprise the binding cavity. Finally, by perturbing the electrostatic charge of both Arg groups (positive → neutral) and the fatty acid headgroup (negative → neutral), we can examine the electrostatic contributions to ligand stabilization. As shown in this report, ALBP has a very stable secondary structure in the presence of the fatty acid ligands; however, there was a noted difference in the motion of the oleate fatty acid headgroup and acyl chain dihedrals, compared to stearate, suggesting that acyl chain motion is affected by presence of a double bond.

METHODS

Preparation. All simulations were performed using Silicon Graphics workstations (R4000, R4400 single processor) and the Insight II/Discover Software Package (version 2.9, BIOSYM, Inc., San Diego, CA). The Brookhaven atomic coordinates for ALBP, in the apo (1lib) and holo forms (stearate, C18:0, 1lif; oleate, C18:1, 1lid) were utilized for the simulations. For each of the three ALBP structures, we modified the partial atomic charges for binding cavity amino acids and/or the fatty acid headgroup in the following way:

Case I: The *charged* forms for the following amino acids lining the pocket were used: Glu72 and Asp76 were represented in the deprotonated, carboxylate form (net charge = −1.00), whereas Arg78, Arg106, and Arg126 were represented in the protonated form (net charge = +1.00). This was accomplished by selecting these protonation states from the BIOSYM residue library. The fatty acids (designated as 132H) were represented in the deprotonated, carboxylate form. No counterions were used with any of the aforementioned side chains. Since we are primarily interested in events within the protein pocket, amino acids exposed to the outer aqueous environment were left neutral. Potential types and partial atomic charges for each form were derived from the CVFF forcefield (Dauber-Osguthorpe *et al*., 1988).

Case II: The *neutral* forms for all amino acids in the pocket were used, and the fatty acids was modeled in the protonated form (charge = 0). No changes in other ALBP amino acids occurred.

The completed six structures (Table 1) were then soaked in a 5 Å layer of water in preparation for simulation; only a slight variation in the number of waters surrounding the these structures was observed. The conserved and solvent water molecules were represented using the CVFF water model, which uses the nonbond parameters of SPC water with the internals of TIP3P model. Since our focus is primarily on events occurring within the binding pocket, our simulations did not require the use of periodic boundary conditions.

Simulations. The CVFF forcefield (Dauber-Osguthorpe *et al*., 1988) was used for Cartesian minimization and MD simulations. Our representation of Coulombic interactions involved the use of a linear distance-dependent dielectric (1**r*) equal to the interatomic separation. A 10 Å cutoff was applied with a spline switching function to smooth pairwise nonbonding interactions to zero within 1.5 Å of our boundary. No cross-terms were used in the energy expression, and a simple harmonic valence potential was used to model the valence bond stretching term. The CVFF forcefield does not use a separate term for hydrogen bonds as in many other forcefields; rather, hydrogen bonds are a consequence of the standard van der Waals and electrostatic parameters (Hagler *et al*., 1979a,b). The choice of forcefield, cutoff, and dielectric value, as well as the extent of water used, was based upon a series of preliminary minimization and dynamics simulations: we selected parameters which produced low RMS deviation from the crystal structures during the course of the simulation (Dagett & Levitt, 1993; Geunot & Kollman, 1993). The CVFF forcefield has previously been used in protein MD simulations (Paulsen *et al.*, 1991; Kitson *et al*., 1993, and references therein) as well as simulations for lipids (Stouch *et al*., 1991; Bassolino-

Table 1: ALBP Variants Utilized in MD Simulations

protein−FA complex	binding pocket conditions[a]	solvation shell[b]	acronym
ALBP, apo form			
charged	(−): E72, D76 (+): R78, R106, R126	837	Apo-C
neutral	all residues neutral	837	Apo-N
ALBP, stearate complex			
charged	(−): E72, D76, 132H (+): R78, R106, R126	837	Stear-C
neutral	all residues + FA neutral	837	Stear-N
ALBP, oleate complex			
charged	(−): E72, D76, 132H (+): R78, R106, R126	860	Oleic-C
neutral	all residues + FA neutral	860	Oleic-N

[a] The listed amino acids (and, where applicable, the fatty acid) were represented either as the charged form [carboxylate, COO^-, (−); guanidino, NH_2^+, (+)] or as the neutral form (COOH, NH). The symbol 132H is used to denote the FA, or fatty acid carboxylate headgroup. [b] Number of water molecules comprising the ALBP solvent shell.

Klimas *et al.*, 1993; Williams *et al.*, 1993). In addition, we have chosen the CVFF Forcefield to remain consistent with our earlier work, and to permit comparisons of results to be made therein (Rich, 1993).

Prior to the dynamics simulations, we performed Cartesian minimization for each of the six protein−ligand complexes in the following manner to relieve bad contacts and "relax" the structures. The following protocol was used: (1) All non-hydrogenic atoms for both protein and solvent were first constrained, and then the hydrogens were allowed to minimize using steepest descent minimization until the maximum derivative $\langle|dE/dr|\rangle$ of the system was <10.0 kcal/(mole·Å). (2) This was followed by constraining only the protein backbone and allowing all other atoms to relax, using the same steepest descent protocol described in (1). (3) The final minimization consisted of relaxing all atoms in the system using conjugate gradient minimization, until the maximum derivative was <0.1 kcal/(mole·Å). The final RMS derivative for all minimized structures was found to be <0.01.

Subsequently, MD simulations were performed using the Verlet leapfrog algorithm with a time step of 1.0 fs. A constant temperature was maintained during the course of the simulation by weakly coupling to a thermal bath (Berendsen *et al.*, 1984). The initial velocities were obtained from a Maxwellian distribution. The system was then slowly warmed to 300 K. After a 10 ps equilibration stage (discard data), the MD was continued for an additional 90 ps. Sampling of data points occurred this interval at every ps. In order to access the efficacy of the 100 ps simulations, two additional simulations were performed for a duratation of 200 ps (10 ps of equilibration followed by 190 ps of sampling). These simulations were performed using only the Stear-C and Oleic-C forms.

MD Data Analysis. Time-dependent protein−lipid interactions were evaluated in several ways. Root-mean-square deviation (RMSD) from the crystal structure for backbone atoms was determined to assist in identifying major protein movement, as was use of RMS deviation between all heavy atoms (including all heavy side-chain atoms). Distances for important hydrogen bonds associated with fatty acid binding, as well as fatty acid acyl torsion angles, were monitored during the course of the MD simulation. For torsional motion, the number of transitions over barriers were obtained from the plots of dihedral angles as a function of time. By definition, a torsional transition was taken as a transition from either *gauche* → *trans* ($g \rightarrow t$), *trans* → *gauche* ($t \rightarrow g$), or *gauche* → *gauche* ($g \rightarrow g$) conformer states. To determine the fraction of *gauche*, we did the following: for each fatty acid complex, we determined the dihedral values for each torsion in the acyl chain and classified that rotamer state as either *gauche* or *trans*. This calculation was performed for each picosecond of the MD simulation, thus yielding a total of 90 conformers sampled. We then determined the *average* ratio of *gauche*-to-*trans* over the entire rotamer population for each fatty acid. We employed this procedure so that our results can be compared with experimentally determined *gauche, trans* populations (Gaber & Peticolas, 1977; Mendelsohn *et al.*, 1989) and other theoretical simulations (Venable *et al.*, 1993; De Loof *et al.*, 1991).

In order to understand the role of water in binding and dynamics of the fatty acid, we measured the mean-square displacement of the water molecules in our system. Time-dependent measurements were performed on the following: (1) all waters molecules in system, including crystallographic and solvent shell; (2) crystallographic water molecules exclusively; (3) the 10 conserved waters (denoted as WAT 1−10, as per the terminology of LaLonde *et al.*, 1994a); and (4) WAT 1 exclusively, defined as the intervening water between Tyr128 and Arg106. Relative diffusion of water in each of the molecular dynamic simulations was determined as plots of mean-square displacement as a function of time.

RESULTS

Minimized and Time-Dependent Structures for Various ALBP Complexes. Using the CVFF forcefield, we first examine the relaxation or perturbation in the 6 ALBP protein structures following Cartesian minimization to convergence (Table 2). We note that the backbone and all-atom RMSD values exhibited a range of 0.57−0.78 and 0.74−0.86 Å, respectively. ALBP−stearate complexes exhibited smaller RMSD values from the crystal structure than either the apo forms or the ALBP−oleate forms. We did not observe any significant discrepancies in the protein backbone and all-atom RMSD values for any of the -N and -C forms (Table 2). No significant structural perturbations were noted for fatty acids in any of the protein−lipid complexes; however, we do observe that the RMSD values for the neutral forms of each fatty acid are 1.5−2 times those obtained for the carboxylate forms. For molecular dynamics simulations, an

Table 2: Comparisons of Crystal, MD, and Cartesian Minimized ALBP Structures

protein complex	backbone RMSD, Å[a]			all-atom RMSD, Å[a]			fatty acid RMSD, Å[a]		
	min[b]	MD[c]	±SD	min[b]	MD[c]	±SD	min[b]	MD[c]	±SD
Apo-N	0.77	0.98	0.05	0.86	1.18	0.07	N/A	N/A	N/A
Apo-C	0.72	0.97	0.07	0.81	1.16	0.05	N/A	N/A	N/A
Stear-N	0.57	0.87	0.05	0.74	1.14	0.07	0.92	0.96	0.11
Stear-C	0.65	0.87	0.04	0.76	1.11	0.04	0.47	0.58	0.10
Oleic-N	0.78	0.97	0.06	0.86	1.21	0.08	0.73	1.13	0.13
Oleic-C	0.74	0.87	0.05	0.75	1.07	0.04	0.52	0.67	0.13

[a] RMSD determined between the Cartesian coordinates of the protein crystal structure and those of the CVFF-determined structures, exclusive of hydrogen atoms. "All-atom" refers to both backbone and side-chain atoms in ALBP. [b] "min" = minimized by the protocol described in the Methods section. Represents a single structure. [c] "MD" = from molecular dynamics simulations, 90 ps trajectory. RMSD is the mean of 90 different structures.

examination of the RMSD values obtained for ALBP structures at picosecond intervals of each trajectory (90 structures total/simulation) reveals similar results (Table 2). During MD simulations the average RMSD was observed to be less than 1 Å for backbone structures and between 1.07 and 1.21 Å for all-atom structures. These values are representative of stable simulations for proteins of this size (Dagett & Levitt, 1993). Interestingly, acyl chain saturation appeared to have a minimal effect on the overall RMSD values (compare Stear- with Oleic- values, Table 2). From these results, we conclude the following: the charge perturbations performed on binding cavity residues E72, D76, R78, R106, R126, and the 132H fatty acid do not lead to significant global structural perturbations in the ALBP protein.

Perturbations in ALBP Secondary Structure Domains. To determine the extent of *localized* conformational change for specific ALBP secondary structure motifs, we plotted the backbone RMSD (MD average structure compared to crystal structure) as a function of residue number (Figures 2 and 3). These comparisons indicate that significant changes are primarily confined to β-turn or loop regions located between β-sheet and/or α-helix domains. The Apo-C form possesses significant conformational fluctuations at the loop regions linking (a) the α2-helix domain and (b) the βE-βF domains which comprise a large opening between the internal cavity and external solvent. The -C forms of ALBP−fatty acid complexes exhibit less pronounced conformational fluctuations; these are localized to the loop regions linking the βG-βH and βF-βG domains for Stear-C and Oleic-C, respectively. In contrast, the -N forms (Figure 3) do not exhibit specific localized fluctuations; rather, they exhibit conformational variability over most of the turn or loop regions within the ALBP protein. These results can be contrasted with earlier MD studies of ALBP−palmitate complexes at 1000 K (Zanotti *et al*., 1994), where similar conformational fluctuations were reported for α-helix II and loop βE-βF; in addition, at this higher simulation temperature, conformational perturbations were also noted for loop βC-βD.

As shown in Figure 1, the crystal structure of the ALBP−fatty acid complex (stearate is shown as an example) reveals that the fatty acid headgroup interacts with two arginine residues, one tyrosine residue, and one water molecule. To understand the role of Arg and Tyr residues in the stabilization of the fatty acid within the binding cavity, we superimposed the locations of Arg106, Arg126, and Tyr128 on the MD RMSD trajectories (Figures 2 and 3; vertical lines indicate the location of each residue on the protein backbone).

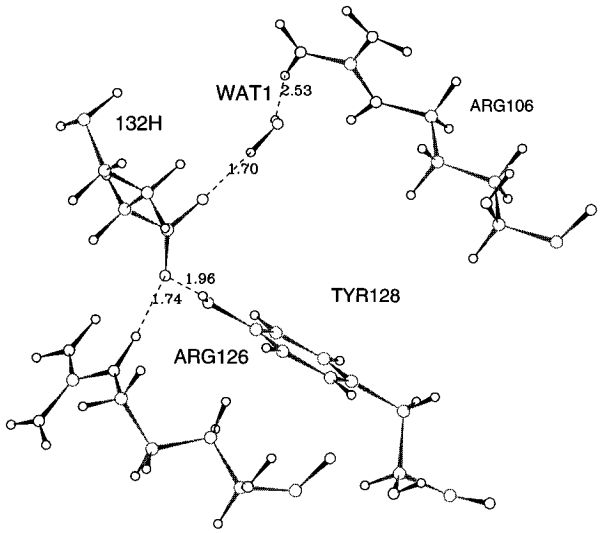

FIGURE 1: X-ray crystal structure of the binding cavity for ALBP−stearate complex. Figure represents the ALBP−stearate crystal structure with hydrogens added and then subject to a short minimization protocol in the CVFF forcefield. Bond distances shown are in Å.

We observe that, over the course of the simulation for Apo-C, Stear-C, and Oleic-C, the time-dependent backbone fluctuations at these locations are very small and do not deviate significantly from the crystal structure (Figures 2 and 3). In addition, we found that the side-chain RMSD for Arg106 and Arg126 in the minimized and MD time-dependent Apo-N, Stear-N and -C, and Oleic-N and -C structures is minimal. Interestingly, Arg126 has been found to exhibit two distinct conformational states in the crystal structure of apo-ALBP (Banaszak *et al*., 1994). The increased motion of the Arg residues within the binding cavity of Apo-C may be the result of charge−charge repulsion between guanidino groups. This was confirmed by monitoring the guanidino−guanidino (carbon−carbon) time-dependent distances (Figures 4a,b). These plots confirm the hypothesis that strong repulsive electrostatic forces exist between positively charged Arg residues within the binding cavity and that the fatty acid carboxylate group stabilizes charge−charge interactions (LaLonde *et al*., 1994b). This electrostatic effect is not observed for either Apo-N or for any of the fatty acid−protein complexes in our study. We conclude that Arg106, Arg126, and Tyr128, in the presence of the fatty acid headgroup, participate in nonbonding interactions which stabilize side-chain and backbone conformational states within the ALBP binding pocket. We have compared the number of hydrogen bonds in the apo charged

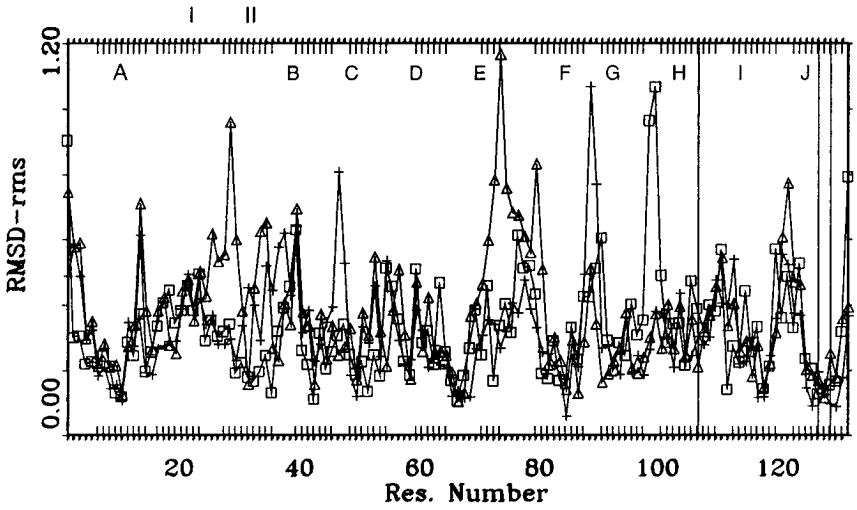

FIGURE 2: Backbone Cartesian coordinate RMS difference (in Å) for crystal and MD-determined ALBP−fatty acid complexes. Apo-C (△), Stear-C (□), and Oleic-C (+). Extended bars are shown at residues Arg106, Arg126, and Tyr128.

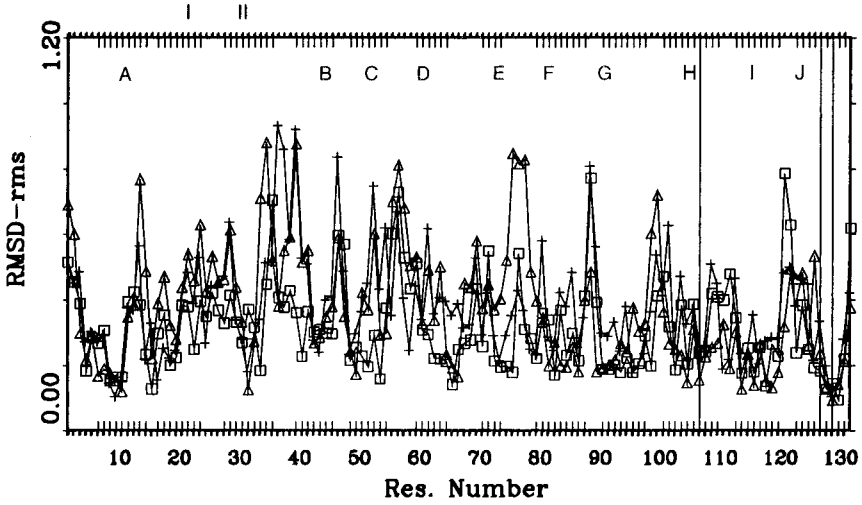

FIGURE 3: Backbone Cartesian coordinate RMS difference (in Å) for the -N complexes. Apo-N (△), Stear-N (□), and Oleic-N (+).

and neutral forms in order to determine if additional hydrogen bonds are present in the neutral form which help stabilize the neutral form over the charged form. There is no significant difference in the *number* of hydrogen bonds during the course of simulation.

Fatty Acid Structure and Dynamics. The RMSD values obtained for stearate and oleate fatty acids in the -N and -C forms are presented in Table 2. We find that, for the minimized ALBP complexes, the RMSD values were 0.47 and 0.92 Å, respectively, for Stear-N and Stear-C, and 0.52 and 0.73 Å for Oleic-N and Oleic-C, respectively. For these minimized -N and -C complexes, we determined the sterate and oleate acyl chain dihedrals in each ALBP−fatty acid complex, using the torsion angle nomenclature for fatty acids of Xu *et al.* (1993) (Figure 5). The -N complexes feature a slightly larger torsional deviation from the crystal structures as compared to the -C complexes. We did not observe any dihedral transitions within the acyl chains for either stearate or oleate fatty acids after minimization (Figure 5).

During MD simulations, the average RMSD values obtained for -C ALBP fatty acid complexes were found to be lower than those obtained for the -N complexes (Table 2). To understand this behavior, we compared the time-dependent conformational fluctuations for each fatty acid. This involved the determination of the following:

(1) The motion of the dihedral headgroup ($O_2-C_1-C_2-C_3$), designated as the C2 torsion. Figure 6 compares the time course for the dihedral headgroup motion for Stear- and Oleic- forms. Generally, oleic acid demonstrated a far greater time-dependent motion of the C2 dihedral than stearic acid. In addition, torsional transitions for C2 were observed during the course of the simulation for Oleic- forms (Figure 6). We observed greater fluctuations in the C2 dihedral for Oleic-N as compared to Stear-N; however, these fluctuations were not as pronounced as for Oleic-C.

(2) The number of dihedral transitions observed along the acyl chain. The observed acyl chain dihedral transitions are shown in Table 3. In addition, Figure 7a,b presents 10 ps interval "snapshot" images for fatty acid conformers. In the case of stearate−protein complexes, most transitions occur at the methyl end of the chain ($C_{12}-C_{16}$) for both the -C and -N forms. Interestingly, the C14 dihedral exhibited a significantly larger number of transitions. For oleate−protein complexes, a greater number of transitions were observed for both -N and -C forms compared with stearate complexes; furthermore, the location of transitions were less specific for oleate complexes (see Table 3). The following points of interest in Oleic- simulations should be noted: (a) For C2, C9, and C11 dihedrals, there is an increase in fluctuations (Figure 6). These angles correspond to the fatty acid head

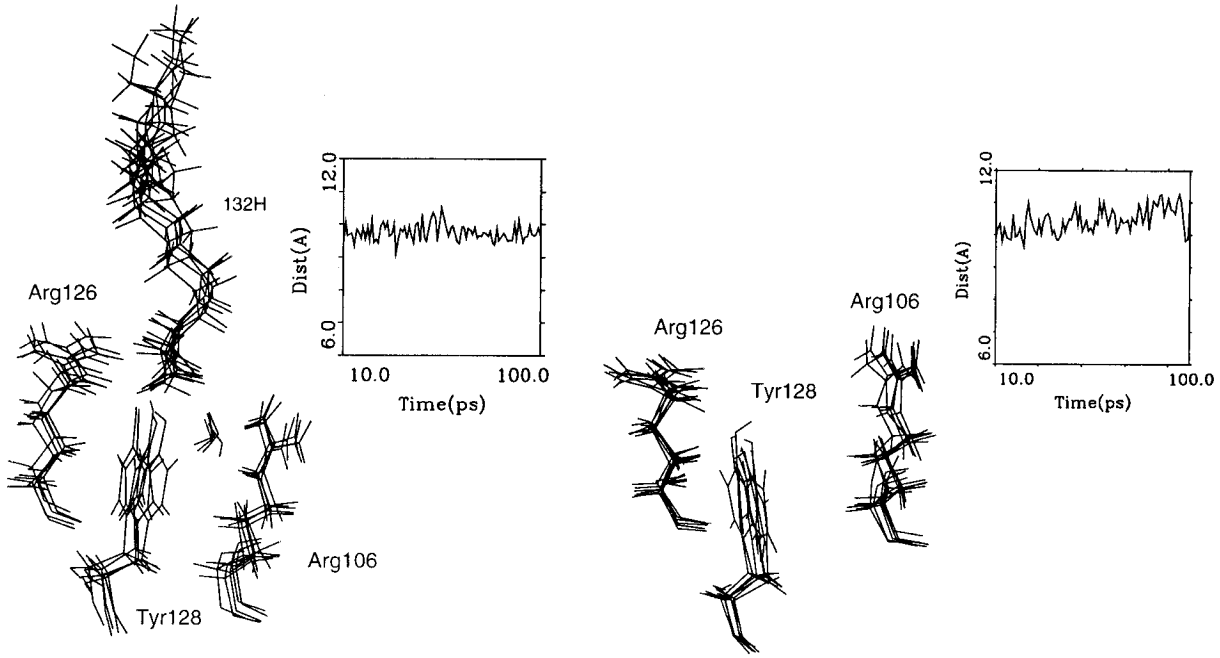

FIGURE 4: Snapshots of Arg106, Arg126, and fatty acid headgroup conformers within the apo-ALBP and ALBP−stearate complex. Side-chain and fatty acid conformers within the binding cavity of the ALBP were extracted from the MD trajectory files (at time intervals of 0, 10, 30, 50, 70, and 90 ps). (a, right) Apo-C; and (b, left) Stear-C. The insets show the distance (Å) as a function of time (ps) between carbon-centered guanidino atoms Arg106−Arg126.

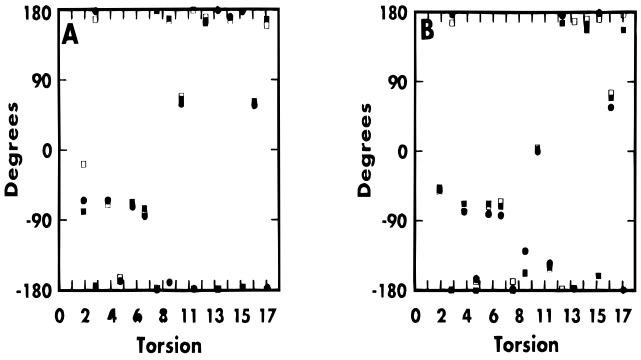

FIGURE 5: Fatty acid acyl chain torsion angles obtained for CVFF-minimized ALBP−fatty acid complexes. (A, left) stearate; (B, right) oleate. (●) Crystal, (■) -C, and (□) -N.

group, and to the two single carbon bonds adjacent to the alkene bond. Since predominant fluctuations are not observed in the C2 dihedral for Stear-C, it is likely that fluctuations in C2 for Oleic-C originate from motion within dihedrals C9 and C11. (b) The *gauch−gauche* configuration associated with the C6, C7 dihedrals was conserved during the course of all MD simulations; the exception being Oleic-C. This $g \rightarrow t$ transition however was followed by $t \rightarrow g$ transition within the same C6 dihedral.

(3) The fraction of rotamers in the gauche state. We found that the fraction of *gauche* rotamers remained relatively constant for both fatty acid−protein complexes during the course of the MD simulation (Table 3). The fraction of *gauche* rotamers was 0.28−0.37 and 0.25−0.31 for stearate− and oleate−ALBP complexes, respectively. Experimentally, the number of *gauche* rotamers/chain has been calculated to be 3.6/chain (0.24) for dipalmitoylphosphatidylcholine (DPPC) (Mendelsohn *et al.*, 1989). Theoretical calculations using a combined approach of molecular and stochastic dynamics, and a mean field based Marcelja model, resulted in an average *gauche* ratio of 0.25 for DPPC (De Loof *et al.*, 1991). Both of these studies were performed above the phase transition for the acyl chain. These values may be compared with the 1 *gauche* bond/chain observed in the "liquid-ordered" state of DPPC/cholesterol mixtures (Davies *et al.*, 1990). Gaber and Peticolis (1977) reported that conformational order in the gel state at 33 °C is very high; only 1.5−3.0% of *gauche* bonds in the 6 and 10 position of the acyl chain were found.

(4) The end-to-end carbon distance (C_1−C_{18}). The end-to-end acyl chain distances in CVFF-minimized Stear-C and Stear-N complexes were found to be 14.7 and 15.3 Å, respectively. This can be contrasted with a value of 13.8 Å for *trans*-stearic acid (Rich, 1993). The average end-to-end distances (during MD simulations) of complexes containing stearic acid were 14.8 and 15.0 Å for the -C and -N forms, respectively, (see Table 3). The end-to-end acyl distances in CVFF-minimized Oleic-C and Oleic-N were found to be 14.4 and 14.3 Å, compared with a value of 14.1 Å for crystalline oleic acid (Rich, 1993). For oleate−protein complexes, we noted a tendency for acyl end-to-end distances to shorten during molecular dynamics simulations. This is reflected in end-to-end values of 13.6 and 13.9 Å during MD simulations.

A Putative Role for Hydrophobic Residues Lining the Pocket. In order to determine the putative role for hydrophobic residues lining the pocket, we compared the time-dependent RMS deviation for Phe16, Tyr19, Met20, Val32, Ala33, and Met40 (heavy atoms only) in the apo and the two holo forms. A significantly lower average RMS deviation (0.44 Å) is found for these residues in the stearate−protein complex, compared with 0.62 Å in the apo and 0.65 Å in the oleic−protein complex. The lower RMS values for the stearic−protein complex may be correlated with a decrease in acyl chain motion for stearic compared with oleic acid: as shown in Table 2, RMS deviations (fatty acid only) of 0.58 Å for Stear-C and 0.67 Å for Oleic-C were obtained. In contrast, there is very little difference between all-atom RMS deviations for the protein structures of Stear-C and

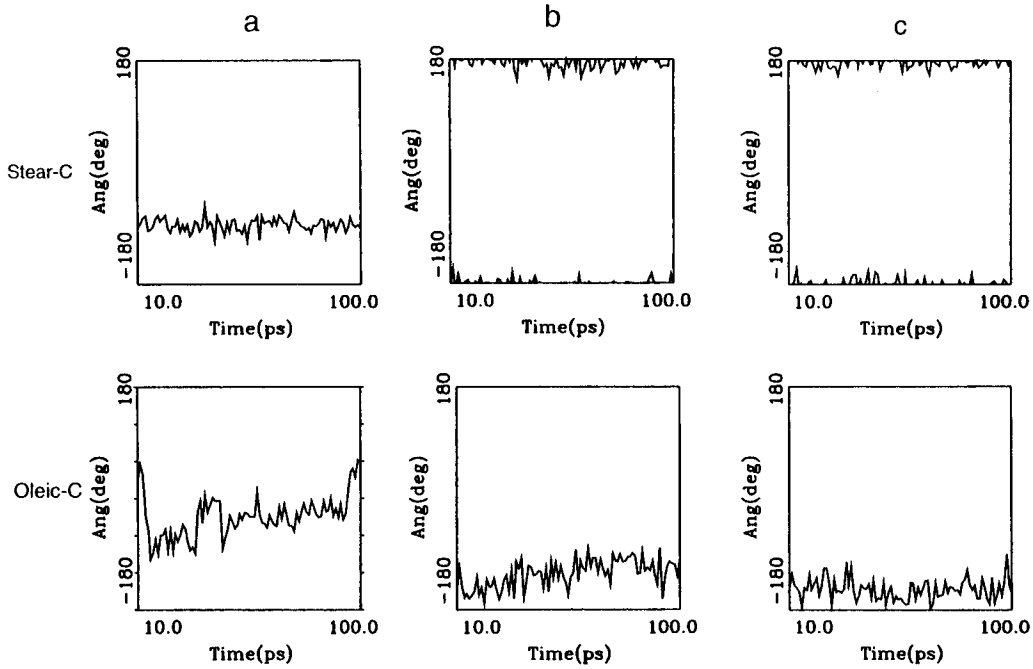

FIGURE 6: Time-dependent fluctuations within dihedral angles. (a) Fatty acid headgroup C2 dihedral ($O_1-C_1-C_2-C_3$), (b) C9 acyl dihedral, and (c) C11 acyl dihedral. Top traces: Stear-C ALBP complex. Bottom Traces: Oleic-C ALBP complex.

Table 3: Comparison of ALBP-Associated Fatty Acid Conformers

	fraction *gauche*[a]	head-to-tail distance, Å[b]	obsd dihedral transitions[c]
stearic−ALBP			
crystal	0.33	13.8	N/A
Stear-N, min	0.33	15.3	N/A
Stear-N, MD[d]	0.28	15.0 (±0.6)	C14 ($t \rightarrow g^-$); C14 ($g^- \rightarrow t$)
Stear-C, min	0.33	14.7	N/A
Stear-C, MD[d]	0.37	14.8 (±0.5)	C14 ($t \rightarrow g^+$)
oleic−ALBP			
crystal	0.31	14.1	N/A
Oleic-N, min	0.31	14.3	N/A
Oleic-N, MD	0.25	13.6 (± 0.7)	C4 ($g^- \rightarrow t$); C11 ($t \rightarrow g^+$); C13 ($t \rightarrow g^-$)
Oleic-C, min	0.31	14.4	N/A
Oleic-C, MD[d]	0.29	13.9 (± 0.5)	C4 ($g^- \rightarrow t$); C4 ($t \rightarrow g^-$); C6 ($g^- \rightarrow t$); C6 ($t \rightarrow g^-$)

[a] Fraction in *gauche* includes dihedral angles C3−C17 within the saturated chain, taken as 15 dihedrals for stearate and 12 for oleate. For oleic acid the region bounded by the double bond (C9−C11) is not included. [b] End-to-end distance between C_1 and C_{18} are the mean values during the MD simulation. Included are the standard deviations. [c] Number of dihedrals corresponds to number of transitions observed during the course of the simulation.

Oleic-C (Table 2). We believe that these results are consistent with our hypothesis that fatty acid motion is primarily dictated by the saturation characteristics of the acyl chain, and that the hydrophobic pocket may play a role in the stabilization of the acyl chain.

Effect on Water Displacement. To gain some insight in determining the role of water in fatty acid binding, we examined the msd of binding pocket water molecules for the three MD simulations performed using the -C form (Figure 8). Each graph shows four plots for the following: (1) all waters (bulk + crystallographic); (2) only crystallographic waters; (3) only the 10 conserved waters; and (4) only WAT1 (i.e., the intervening water between 132H and Arg126). The behavior of all water molecules is relatively consistent between simulations with the exception of Oleic-C. The lower msd found for the Oleic- simulations (for all waters) is most likely the result of a greater number of water molecules present in the 5 Å shell surrounding the protein (see Table 1). For all simulations the lower msd observed for crystallographic waters (compared with all waters) is consistent with results of Wong and McCammon (1986): the diffusion rate of water is dependent on the distance from the protein; the closer the water is to the protein, the less the diffusion rate. The 10 conserved waters located within the binding pocket had lower msd values than all crystallographic waters, the exception being Apo-N, where there appeared to be little difference in msd between all crystallographic and the 10 conserved waters. This indicates that the polar residues found within the cavity can restrict the motion of internal water molecules. Figure 8 also shows the msd for WAT1 to be markedly lower in all protein complexes, including Apo-C.

Comparison of 100 versus 200 ps MD Simulations Using Stear-C and Oleic-C. In order to access the efficacy of the 100 ps simulations, 200 ps simulations were performed on Stear-C and Oleic-C complexes. There was virtually no change in the ALBP protein RMS deviation (backbone and all-heavy) between 100 and 200 ps; the final RMSD for all backbone was found to be 0.92 and 0.94 for Stear-C and Oleic-C protein−fatty acid complexes, respectively. The 200 ps dynamic behavior of the fatty acids in the binding cavity was found to be similar to the 100 ps simulations. Specifically, acyl chain motion and dihedral transitions were more pronounced in Oleic-C as compared wih Stear-C, and the limited transitions in Stear-C were observed in the tail end compared to a more uneven distribution in Oleic-C. Oleic-C demonstrated two transitions in the C2 headgroup during the 200 ps simulation. Surprisingly, we did observe *one* acyl C2 torsional transition for Stear-C during the 200 ps simulation. This single observed C2 transition in Stear-C occurred simultaneously to transitions at C4, C14, and C16. This was the only stearate headgroup transition observed in the total 400 ps of simulation for Stear-C; we did not observe any C2 transitions during the 100 ps simulations.

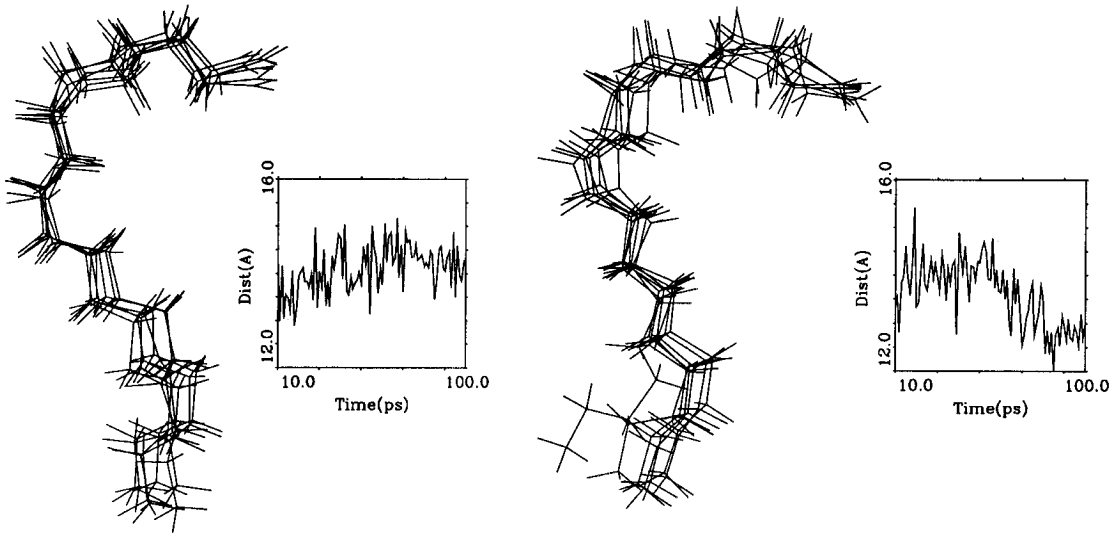

FIGURE 7: Snapshots of ALBP-associated fatty acid conformers. Structures within the binding cavity of the charged forms of the ALBP−fatty acid complexes were extracted from the MD trajectory files (at time intervals of 0, 10, 30, 50, 70, and 90 ps). (a, left) Stear-C; (b, right) Oleic-C. Insets show plots of the end-to-end (C_1-C_{18}) carbon distances (in Å) during the course of the simulation.

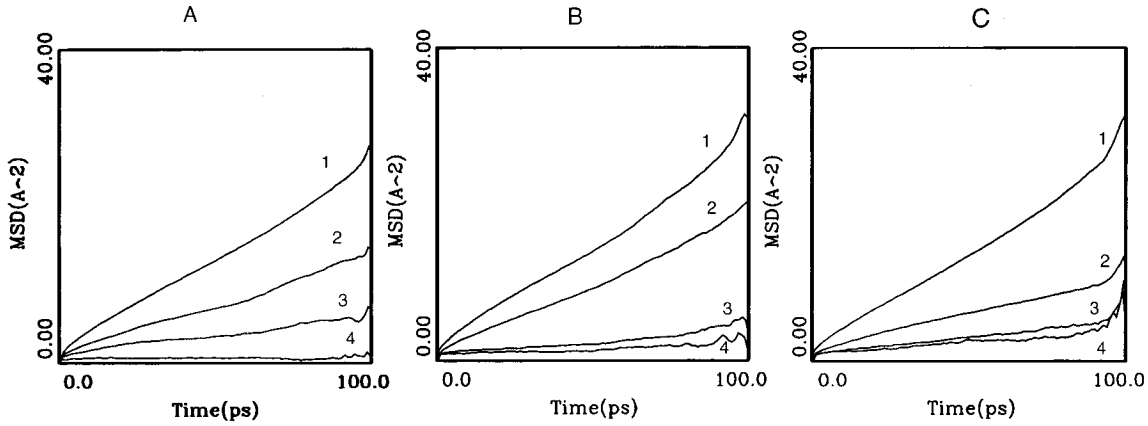

FIGURE 8: Relative displacement of water molecules during MD simulations. (A) Apo-C, (B) Stear-C, and (C) Oleic-C ALBP complexes. In each graph, the traces running from top to bottom are as follows: (1) all waters; (2) all crystallographic waters; (3) crystallographic waters contained within the FABP pocket; and (4) WAT1, the intervening water between residues 132H and Arg106.

DISCUSSION

Role of Electrostatics on ALBP-FA Stabilization. The results from our MD simulations support the view that ALBP is a highly stable protein exhibiting only small perturbations in its β-barrel structure over 100 and 200 ps (Figures 2 and 3; Table 2). This is consistent with MD studies which demonstrate a high degree of stability in β-sheet regions of protein (see Vijayakumar & Beveridge, 1994, and references therein). Of considerable interest is the binding pocket of ALBP, which contains Arg106, Arg126, and Tyr128. This region shows a very high degree of backbone and side-chain stability, as evidenced by the low rms factors observed for Apo-N, Stear-C/N, and Oleic-C/N complexes during the course of our MD simulations (Figures 2 and 3). These results are consistent with the low temperature factors observed in the crystal structure for this region with the exception of Arg126 in the apo-ALBP, which has a dual conformation in the crystal structure (Xu *et al.*, 1993).

The fatty acid headgroup is stabilized via interactions with Arg106, 126, Tyr128, and one water molecule (Banaszak *et al.*, 1994; Xu *et al.*, 1993). The stabilizing role of Arg residues in protein−lipid interactions was demonstrated in experimental studies involving site-directed FABP mutants featuring arginine deletions; in these mutant proteins, lipids are bound with much lower affinity (Jakoby *et al.*, 1993). The contribution of the guanidino charge to the stability of these complexes is undoubtedly an important one, as shown in Figure 4a,b. Here we demonstrate that, within the binding pocket of Apo-C, a strong repulsive interaction is present between the two charged arginines. The introduction of a fatty acid into the apo-ALBP binding pocket was found to stabilize the repulsion between Arg106 and Arg126. We conclude that ALBP guanidino electrostatic interactions are a significant contributor to the binding energy in the -C protein−fatty acid complexes. These findings are consistent with other studies: (1) database analyses which demonstrate the importance of Arg electrostatic interactions on protein tertiary folding and stability (Mrabet *et al.*, 1992; Nandi *et al.*, 1993; Flocco & Mowbray, 1994); and (2) calorimetric studies that show almost 90% of the ALBP−fatty acid binding energy being enthalpic, containing an electrostatic, and to a lesser extent, a van der Waals component (LaLonde *et al.*, 1994b). Note that our MD results only examine lipid when bound to the protein and do not consider the differential energy components that may exist as a result of differences in lipid solubility between protein and water phases (see Richieri *et al.*, 1994, and references therein). In addition, we should point out that hydrogen bonding interactions

would be another significant stabilizing force for fatty acid carboxylate−guanidino interactions (Nandi *et al.*, 1993). Thus, experimental studies, database information, and theoretical simulations support the view that the arginine guanidino group plays an important role in fatty acid headgroup stabilization with the ALBP binding cavity.

A Putative Role for Crystallographic Waters in Fatty Acid Binding Pocket Interactions. As shown in Figure 8, the 10 conserved waters in the binding pocket do not exhibit noticeable diffusion during the course of our MD simulations on ALBP−fatty acid complexes. This is particularly true for WAT1, which participates in the hydrogen bonding complex that is responsible for fatty acid headgroup stabilization. The only exception was observed for the Apo-N ALBP protein, where the diffusion of the 10 conserved waters approximated that of the other crystallographic waters outside the binding cavity (Figure 8). From these observations, we surmise that the presence of charged and polar amino acid side chains within the binding cavity is a significant factor in retaining these water molecules. Noting that there is an absence of counterions within the binding cavity (Banaszak *et al.*, 1994), we propose that these side-chain-associated water molecules may play a role in shaping the electrostatic environment within the cavity, thereby creating a stabilizing attractive force for fatty acid binding.

Dynamics of the Fatty Acid Headgroup and Acyl Chain. In the crystal and minimized ALBP−fatty acid complexes, we find that only minor differences exist between oleic and stearic acid acyl chain conformations (Figure 5). However, the most important difference between the two fatty acids is the degree of *motion* (Figures 6 and 7; Table 3). Given that the ALBP binding cavity volume is large (600 Å^3), it is reasonable to suggest that there is enough space to accommodate movement of a fatty acid and, also, permit the movement of side-chain groups which particpate in the hydrogen bonding/electrostatic complex with the fatty acid head group. The combination of these effects would permit fluctations and transitions to occur for a fatty acid headgroup while bound within the ALBP cavity. *What is notable is that unsaturated fatty acids exhibit more motion than saturated fatty acids in the ALBP complex.* We observe this phenomenon on two levels: headgroup-specific motion and acyl chain dihedral transitions (Figures 6 and 7; Table 3). During the course of our MD simulations, it is evident that there is significant headgroup motion observed for oleic acid as compared with stearic acid (Figure 6). Similar observations have been made by Slater *et al.* (1993) where acyl chain unsaturation was demonstrated to have an increased effect on headgroup disorder within bilayer membrane systems. The dihedral transition rates were also found to be different for the acyl chain of Stear- and Oleic- ALBP complexes. Transitions in Stear- ALBP complexes were confined primarily to the end methyl dihedrals (Table 3). This phenomenon was also observed in experimental and MD studies of lipid bilayers containing saturated fatty acids, wherin a tendency for increased disorder toward the methyl group was observed (De Loof *et al*., 1991; Venable *et al*., 1994). In contrast to the stearate findings, we observed a greater number of transitions for oleic−ALBP complexes *which were not limited to the end methyl region* (Table 3). One plausible explanation for this descrepancy in dihedral transition rates is that *the presence of an alkene bond within the acyl chain affects the rotation rates for unsaturated carbon−carbon rotamers.* Support for this hypothesis can be found in recent studies on C-C dihedrals which flank alkene bonds in unsaturated lipids; these rotamers have increased flexiblity compared to alkane bonds in saturated lipids (Wiener & White, 1992a,b). In addition, other studies have shown that C-C rotamers which flank alkene bonds in the acyl chain exhibit increased RMS values (Heller *et al.*, 1994). Hence, the presence of the alkene bond influences the rate of C-C rotamer transitions; these rates, in turn, have an effect on protein−lipid stabilization. One would predict that acyl chain motion and FABP−fatty acid stability would be affected by further addition of alkene units to the acyl chain. To test this hypothesis, MD studies on polyene acyl chain fatty acids (arachidonic, C20:4) are currently in progress.

How do the transition rates obtained for ALBP-associated oleic and stearate fatty acids compare with other theorectically- and experimentally-determined values? The transition rates obtained for both fatty acids in our present study (Table 3) are substantially lower (i.e., more than 1 order of magnitude) than values obtained for free fatty acids *in vacuo* (Rich, 1993).

Higher acyl chain dihedral transition rates (i.e., 1 order of magnitude) were observed in palmitic DPPC bilayers and bulk hexadecane at 50 °C; however, we should note that these studies were performed well above the respective phase transition temperatures, where one would expect the rates to be higher (Venable *et al.*, 1993). However, a more meaningful comparison can be made with data obtained for other protein−lipid MD simulations: our transition rates are comparable with the *in vacuo* results obtained for a 176 ps MD simulation of bovine pancreas phospholipase containing *n*-dodecylphosphorylcholine (Tomoo *et al.*, 1994). Thus our findings are qualitatively consistent with other MD simulations of protein−lipid complexes.

SUMMARY

(1) The β-sheet structure of FABP was found to be highly stable and independent of the bound FA. Incorporation of a charged FA was found to stabilize the interior pocket, in part by reducing the Arg−Arg repulsion observed within the Apo-C pocket. We presume that hydrogen bonding and electrostatics stabilize the ligand−protein complex; however, other factors, such as hydrophobicity, may also play a role in stabilization.

(2) Conserved water movement within the cavity of -C forms was found to be limited and can be attributed to water−side chain interactions. These conserved waters may play a role in defining the electrostatic environment of the binding cavity.

(3) The motion of the FA during MD simulations was found to be independent of electrostatics; both headgroup and acyl motion were determined by the presence of an alkene bond within the acyl chain, with the acyl chain transition rate being less in stearate than oleate.

(4) Our studies support the view that C-C rotamers adjacent to the acyl alkene bond affect the motion within the acyl chain and the headgroup of the fatty acid. This motion in unsaturated FA's may be a determining factor in the binding to FABP's.

ACKNOWLEDGMENT

The authors would like to thank the New York Academic Computing Facility for the use of their facilities in performing these simulations. J.S.E. acknowledges a Young Investigator Award from the Whitaker Foundation.

REFERENCES

Abramson, S. B., Leszczynska-Piziak, J., & Weissmann, G. (1991) *J. Immunol. 147*, 231−236.
Banaszak, L., Winter, N., Xu, Z., Bernlohr, D. A., Cowan, S., & Jones, A. T. (1994) *Adv. Protein Chem. 45*, 89−151.
Bassolino-Klimas, D., Alpiers, H. E., & Stouch, T. R. (1993) *Biochemistry 32*, 12624−12637.
Berendsen, H. J. C., Postma, J. P. M., van Gunsteren, W. F., DiNola, A., & Haak, J. R. (1984) *J. Chem. Phys. 81*, 3684−3690.
Bienvenue, A., Bloom, M., Davis, J. H., & Devaux, P. F. (1982) *J. Biol. Chem. 257*, 3032−3037.
Cremel, G., Fickova, M., Klimes, I., Leray, C., Leray, V., Meuillet, E., Roques, M., Staedel, C., & Hubert, P. (1993) *Ann. N.Y. Acad. Sci. 683*, 164−171.
Daggett, V., & Levitt, M. (1993) *Annu. Rev. Biophys. Biomol. Struct. 22*, 353−380.
Dauber-Osguthorpe, P., Roberts, V. A., Osguthorpe, D. J., Wolff, J., Genest, M., & Hagler, A. T. (1988) *Proteins: Struct., Funct. Genet. 4*, 31−47.
Davies, M. A., Schuster, H. F., Brauner, J. W., & Mendelsohn, R. (1990) *Biochemistry 29*, 4368−4373.
De Loof, H., Harvey, S. C., Segrest, J. P., & Pastor, R. W. (1991) *Biochemistry 30*, 2099−2113.
Fattal, D. R., & Ben-Shaul, A. (1994) *Biophys. J. 67*, 983−995.
Flocco, M. M., & Mowbray, S. L. (1994) *J. Mol. Biol 235*, 709−717.
Gaber, B. P., & Peticolas, W. L. (1977) *Biochim. Biophys. Acta 465*, 260−274.
Guenot, J., & Kollman, P. A. (1993) *J. Comput. Chem 3*, 295−311.
Hagler, A. T., Lifson, S., & Dauber, P. (1979a) *J. Am. Chem. Soc. 101*, 5122−5130.
Hagler, A. T., Dauber, P., & Lifson, S. (1979b) *J. Am. Chem. Soc. 101*, 5131−5141.
Heller, H., Schaefer, M., & Schulten, K. (1993) *J. Phys. Chem. 97*, 8343−8360.
Jakoby, M. G., Miller, K. R., Toner, J. J., Bauman, A., Cheng, L., Li, E., & Cistola, D. P. (1993) *Biochemistry 32*, 872−878.
Kitson, D. H., Avbelj, F., Moult, J., Nguyen, D. T., Mertz, J. E., Hadzi, D., & Hagler, A. T. (1993) *Proc. Natl. Acad. Sci. U.S.A. 90*, 8920−8924.
LaLonde, J. M., Bernlohr, D. A., & Banaszak, L. J. (1994a) *Biochemistry 33*, 4885−4895.
LaLonde, J. M., Levenson, M. A., Rose, J. J., Bernlohr, D. A., & Banaszak, L. J. (1994b) *J. Biol. Chem. 269*, 25339−25347.
Levitt, D. G., & Banaszak, L. J. (1992) *J. Mol. Graphics 10*, 229−234.
Maple, J. R., Dinur, U., & Hagler, A. T. (1988) *Proc. Natl. Acad. Sci. U.S.A. 85*, 5350−5354.
McPhail, L., Clayton, C. C., & Snyderman, R. (1984) *Science 224*, 622−626.
Mendelsohn, R., Davies, M. A., Brauner, J. W., Schuster, H. F, & Dluhy, R. A. (1989) *Biochemistry 28*, 8934−8939.
Mrabet, N. T., Van den Broeck, A., Van den brande, I., Sanssens, P., Laroche, P., Laroche, Y., Lambeir, A.-M., Matthijssens, G., Jenkins, J., Chiadmi, M., Tilbeurgh, H. V., Rey, F., Jannin, J., Quax, W. J., Lasters, I., De Maeyer, M., & Wodak, S. J. (1992) *Biochemistry 31*, 2239−2253.
Nandi, C. L., Singh, J., & Thornton, J. M. (1993) *Protein Eng. 6*, 247−259.
Ohishi, H., Fujii, S., Tomoo, K., Ishida, T., Ikeda, K., Tanabe, K., & Kitamura, K. (1993) *J. Biochem. 114*, 210−214.
Paulsen, M. D., & Ornstein, R. L. (1991) *Proteins: Struct., Funct. Genet. 11*, 184−204.
Rich, M. (1993) *Biochim. Biophys. Acta 1178*, 87−96.
Richieri, G. V., Ogata, R. T., & Kleinfeld, A. M. (1994) *J. Biol. Chem. 269*, 23918−23930.
Slater, S. J., Ho, C., Taddeo, F. J., Kelly, M. B., & Stubbs, C. D. (1993) *Biochemistry 32*, 3714−3721.
Stouch, T. R., Ward, K. B., Altieri, A., & Hagler, A. T. (1991) *J. Comput. Chem. 12*, 1033−1045.
Tomoo, K., Ohishi, H., Ishida, T., Masatoshi, I., Ikeda, K., Sumiya, S., & Kitamura, K. (1994) *Proteins: Struct., Funct. Genet. 19*, 330−339.
Veerkamp, J. H., Peeters, R. A., & Maatman, R. G. H. J. (1991) *Biochim. Biophys. Acta 1081*, 1−24.
Venable, R. M., Zhang, Y., Hardy, B. J., & Pastor, R. W. (1993) *Science 262*, 223−225.
Vijayakumar, Vishveshwara, S., Ravishanker G., & Beveridge, D. L. (1993) *Biophys. J. 65*, 2304−2312.
Wiener, M. C., & White, S. H. (1992a) *Biophys. J. 61*, 428−433.
Wiener, M. C., & White, S. H. (1992b) *Biophys. J. 61*, 434−447.
Williams, D. E., & Stouch, T. R. (1993) *J. Comput. Chem. 14*, 1066−1076.
Wong, C. F., & McCammon, J. A. (1986) *Isr. J. Chem. 27*, 211−215.
Xu, Z., Bernlohr, D. A., & Banaszak, L. J. (1992) *Biochemistry 31*, 3484−3492.
Xu, Z., Bernlohr, D. A., & Banaszak, L. J. (1993) *J. Biol. Chem. 268*, 7874−7884.
Zanotti, G., Feltre, L., & Spadon, P. (1994) *Biochem. J. 301*, 459−463.

BI951574X